MICRO-MECHANICAL SIMULATION OF MODE I INTERLAMINAR FRACTURE IN PARTICLE-TOUGHENED INTERLAYERS

G. Borstnar[1], M.Jackson[2], M.N. Mavrogordato[1], I.Sinclair[1] and S.M. Spearing[1]

[1] Faculty of Engineering and the Environment, University of Southampton, UK,
S.M.Spearing@soton.ac.uk, http://www.southampton.ac.uk/
[2] Solvay, Tempe, AZ, United States, http://www.solvay.com

Keywords: Carbon Fibre Reinforced Polymer, Delamination, Computed Tomography, Finite Element Modelling

ABSTRACT

Time-resolved Synchrotron Radiation Computed Tomography (SRCT) has been used to capture Mode I delamination propagation in particle-toughened Carbon Fibre Reinforced Polymers (CFRPs). 2D plane-strain image-based Finite Element (FE) models were initialised using 'physically representative' particle distributions, where the bulk materials and constituent interfaces of the particle-resin and fibre-resin could be defined. A number of parametric studies showed that the crack path through the interlayer could be altered through controlling the relative strengths of the competing crack paths. Uniquely, the time-resolved SRCT data permitted the simulated crack paths to be compared to experimental results, illustrating a potential path through which more complex 3D FE simulations may be validated against experimental results in the future. Future models will also need to account for the visco-elastic/visco-plastic properties of the resin, as evidenced in the SRCT results, where thin epoxy bridging-ligaments are shown to be capable of substantial deformation across the crack flanks.

1 INTRODUCTION

Out-of-plane low velocity impacts have been shown to significantly reduce the mechanical properties of Carbon Fibre Reinforced Polymers (CFRPs), which is of concern for primary aerospace structures [1]. It has been shown that secondary-phase thermoplastic particles dispersed within interlaminar regions can be used to suppress the spread of delaminations under impact [2]. Although particle-toughened CFRPs can be found in aircraft in service today, there is a still a lack of understanding surrounding how the optimal properties of these interlayers can be achieved. In order to better understand crack initiation and propagation within these interlayers, *in situ* non-destructive imaging of the sequence of crack tip failure processes was captured using Synchrotron Radiation Computed Tomography (SRCT). The results have been used to increase the understanding surrounding the effects of variables such as; particle type, local particle volume fraction and particle size (all to a certain extent within the manufacturer's control), on the local fracture micro-mechanisms and crack path [3], [4]. Understanding and modelling the crack path is important because it has been shown experimentally that the crack growth resistance can decrease when the crack path deviates from the toughened interlayer to the fibre interfaces [5], [6].

Currently, modelling the crack path in these toughened interlayers is underdeveloped. While the authors' previous modelling efforts have tackled simplified local microstructures in the form of one-dimensional (1D) 'particles' [7], this work presents more complex image-based Finite Element (FE) models derived from the SRCT data, with the simulated 2D crack paths compared against the actual crack paths under a (Mode I) double cantilever beam (DCB) load. Simulating crack propagation for particle-toughened interlayers is challenging because a highly discontinuous process zone can form rather than a clearly defined crack tip [2], [3], requiring models to account for bifurcating and merging micro-cracks. Xie and Koslowski [8] tackled this using the phase field damage model in order to capture the discontinuous behaviour in an idealised particle distribution; identifying the effects of

particle-depleted regions, the stiffness of the particles and the relative surface energies of the competing crack paths on the eventual crack path within the toughened interlayer. However, in this work, crack propagation was achieved through the inclusion of bulk resin elements defined with a maximum principal stress (MAXPS) failure criteria, while the fibre and particle interfaces were modelled as elastic contacts with a maximum failure stress. Overall, these simulations have the ability to provide insight into the properties that govern damage propagation within these materials, especially for interrogating variables that are more difficult to physically control by manufacturers.

2 METHOD

2.1 Materials

Proprietary and developmental CFRPs were manufactured by Solvay and cured according to a standard aerospace cycle. 16-ply uni-directional panels were laid up with a 40 μm thick Polytetraflouroethylene (PTFE) insert placed at mid-plane along one edge of the plate. Specimens were cut from the manufactured panels into 2.5 mm (wide) x 3.0 mm (thick) x 120 mm (long) geometries, with the small cross-section chosen in order to maximize the transmission of low energy photons. The material presented in this work had secondary-phase thermoplastic particles dispersed within the interlayer at a 13 % volume fraction (pre-cure value), with an epoxy bulk resin and an intermediate modulus carbon fibre as the primary reinforcement.

2.2 SRCT experiments

A purpose built *in situ* loading device was used to drive a wedge into the mid-plane of the CFRP samples at the insert in order to generate the Mode I opening loads. The crack was initially extended about 5 mm from the end of the insert, following which the specimen was scanned. Afterwards, the wedge was driven further into the sample in a displacement-controlled manner, extending the crack further. The same regions in the specimen were then scanned again, permitting the crack growth to be captured in 3D *in situ*. The experiments were conducted at the Swiss Light Source on the TOMCAT beamline at the Paul Scherrer Insitut, Villigen, Switzerland. A voxel resolution of 0.325 μm was used, with a detector size of 2560 x 2160 pixels. 1501 projections were taken at an exposure of 150 ms for the 180-degree rotation. A beam energy of 15 kV was used, while a propagation distance of 23 mm emphasized the edges between materials of similar attenuation via phase-enhance contrast [9]. The CT data was reconstructed using the in-house GRIDREC method [10].

2.3 Image-based modelling

The 2D plane-strain model was meshed in Abaqus FEA version 6.14 (Dassault Systemes, Velizy-Villacoublay, France) following digital segmentation of the particles from the resin in ImageJ (W. Rasband, Bethesda, Maryland, USA, 2012). The binarised image could be imported into Abaqus as a sketch, where splines could be used to capture the geometry of the particles. The mesh was formed of CPS4 and CPS3 element types, which could then be imported into MultiMechanics version 2016.06.11 (Omaha, NE, USA, 2016) via an input file. A mesh refinement study considered element sizes of approximately 1, 5 and 10 μm, with good agreement in the crack paths between the 1 and 5 μm meshes. In the presented work, the finest 1 μm mesh was used. The total length of the DCB model was 1.5 mm, with the loading points 0.25 mm away from the region of interest (ROI) as shown in Figure 1. Nodes at the ends of both sides of the DCB arms were selected as loading points, and a wedge shaped region of resin was removed from the interlayer in order to facilitate damage initiation in the centre of the 30 μm thick interlayer. The ROI microstructure was determined according to Figure 2, which allowed the crack path to be compared to the experimental one. The baseline properties of the model are shown in Table 1, where the MAXPS criteria for resin failure allowed the crack to propagate in any direction without *a priori* knowledge.

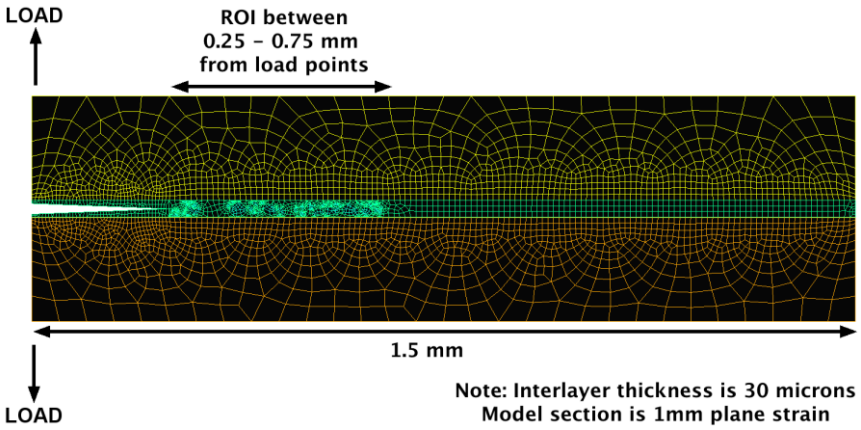

Figure 1: 2D interlayer model geometry and loading conditions (coarse mesh shown for clarity)

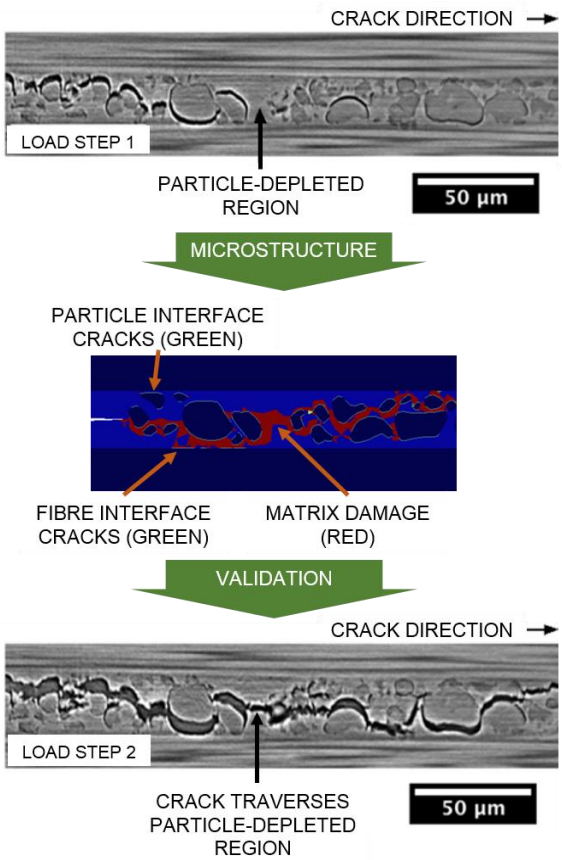

Figure 2: Schematic showing the incorporation of a SRCT-derived microstructure into a 2D FE simulation of Mode I crack propagation within the toughened interlayer

Table 1: Finite element model properties (*Defined by a Prony series, but essentially linear-elastic)

Constituent	Material Model	Stiffness (MPa)	Failure criteria (MPa)
Resin	*Linear-visco-elastic	~3,000	100 (MAXPS)
Ply	Isotropic linear-elastic	150,000	-
De-bonding particles	Isotropic linear-elastic	1,400	-
Fibre interface	Elastic contact	-	60, 70, 80
Particle interface	Elastic contact	-	20, 40, 60

3 RESULTS

The following section presents the modelling results of the 2D plane-strain simulations. Undamaged resin is shown in blue, while the failed resin elements are coloured red. Interface cracks along the fibre-resin and particle-resin interfaces are indicated by the green coloured lines. For clarity, the neighbouring plies and toughening particles are shown in grey. The neat resin failure criteria, ply and particle stiffness's remained consistent in the parametric studies.

3.1 Fibre interface strength effects

In this section, the fibre interface strength was varied from 90 to 60 MPa, while the particle interface strength was maintained at 40 MPa. Figure 3 (a), (b) and (c) show the simulated crack paths for fibre interface strengths of 60, 70 and 80 MPa respectively. The results show that in the presence of the particle-depleted region, the fibre interface will fail when its' strength is 60 MPa and below. As the fibre interface strength was increased to 70 MPa and beyond, the crack path changed and traversed the neat resin as supported by the experimentally determined crack path (Figure 2). As the fibre interface strength was increased further, the smaller isolated instances of fibre interface failure were less common, consistent with expectations. Chronologically, the fibre interface failed prior to the crack path propagating towards it in the 60MPa case, which is consistent with the idea that the crack path is initiation controlled, supporting previous modelling results [7]. These simulations indicate that particle de-bonding ahead of the contiguous crack tip may facilitate failure through the middle of the interlayer, even for lower fibre interface strengths, provided that the distribution of particles is uniform.

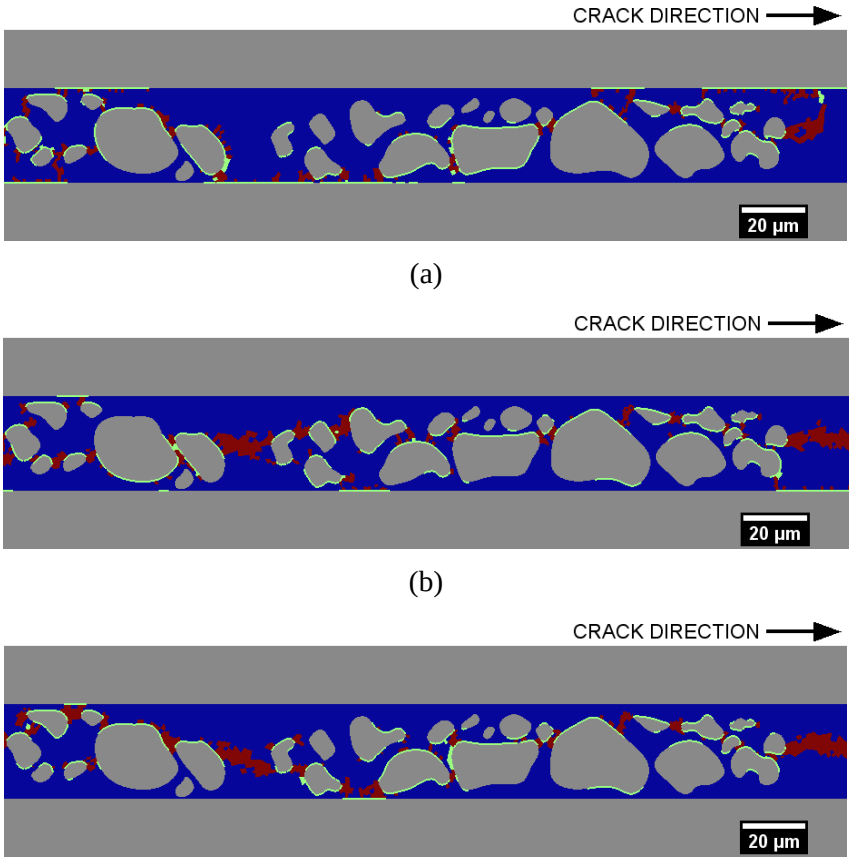

Figure 3: Simulated crack paths for fibre interface strengths of; (a) 60 MPa, (b) 70 MPa, and (c) 80 MPa, showing a change in crack path in the presence of a small particle-depleted region as the fibre interface strength is increased

3.2 Particle interface strength effects

The following section investigated the effects of the particle interface strength on the crack path, simulating the differences in the de-bonding characteristics of the two particle types presented in Borstnar *et al.* [3], where one particle type readily de-bonded and maintained an interlaminar crack path, while the other remained adhered to the resin and resulted in the crack path propagating along the fibre interfaces. Figure 4 shows the simulated crack path for particle interface strengths of; (a) 20 MPa, (b) 40 MPa, and (c) 60 MPa, while maintaining a consistent fibre interface strength of 80 MPa. As expected, the figures show that the extent of the particle de-bonding was reduced as their adhesion to the surrounding resin was increased. Figure 4(b) shows that when the particle interface strength was 40 MPa, two new instances of fibre interface failure occurred while the crack path through the neat resin was also altered. As the particle interface was further increased to 60 MPa, the crack path that initially traversed the neat resin in the particle-depleted region this time deviated to the fibre interfaces (shown in Figure 4(c)). The extent of fibre interface failure was also increased throughout the ROI. Remembering that the resin MAXPS failure criteria was 100 MPa, such an increase in the particle interface strength reduced the amount of diffuse micro-cracking ahead of the crack tip and resulted in a less competitive crack path through the interlayer. Such trends support the previous modelling results presented in [7], where the simulations additionally showed that an increased proximity of a particle to the fibre interfaces will increase the probability of the fibre interface failing. This may explain the instance of fibre interface failure along the bottom of Figure 4(b), where a deviation of crack path (comparing (a) and (b)) to the 'lower' particle after the particle-depleted region may have triggered this event.

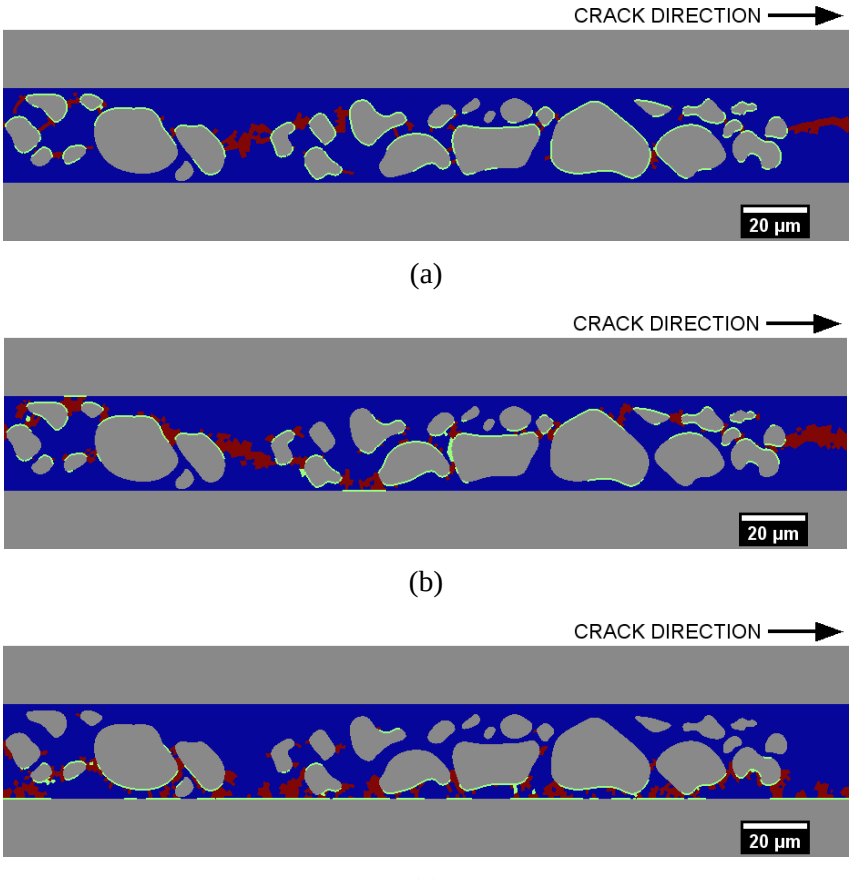

Figure 4: Simulated crack paths for particle interface strengths of; (a) 20 MPa, (b) 40 MPa, and (c) 60 MPa, showing a change in crack path in the presence of a small particle-depleted region as the particle interface strength is increased

3.3 Particle distribution effects

In this study, the effects of local non-uniform particle distributions have been investigated using a different SRCT scan location within the same specimen. A large particle-depleted region (shown in Figure 5(a)) was progressively reduced in size by moving the group of particles on the left hand side, towards the right hand side in 2 μm steps. Figure 5(b) shows that when the particles were moved by 6 μm, that the crack path could traverse the neat resin completely without any instances of fibre interface failure. This transition occurred between the 4 and 6 μm, showing that a reduction in the particle-depleted region size by only 2 μm was enough to change the crack path, evidencing the sensitivity of the crack path to the local microstructure. The chronology of the damage progression supported the previous observations in Figure 3, where the fibre interface failed prior to the crack path growing towards it. These simulations also showed that the crack could also propagate 'backwards' from the particles on the right hand side into the particle-depleted region.

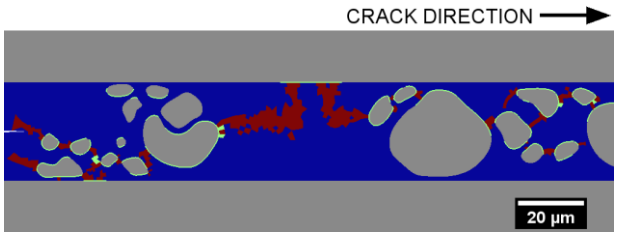

(a)

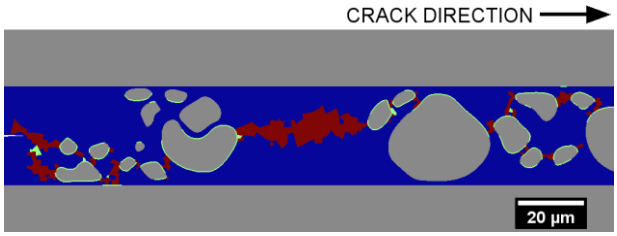

(b)

Figure 5: Showing the effects of reducing the size of the particle-depleted region on the crack path, featuring; (a) the original SRCT-derived microstructure, and (b) moving the group of particles on the left 6 μm to the right

4 DISCUSSION

There are a number of limitations that need to be acknowledged for these models. One of the key limitations is that the models are simulating a 2D plane-strain case, which is illustrated in Figure 6(a). This is not representative of reality and will also limit the crack path from being able to deflect around outstanding intact resin ligaments in the out-of-plane direction. In the experiments, large numbers of resin bridging-ligaments have been evidenced by SRCT *in situ*, which also showed that the crack could also propagate locally in a non-uniform manner, owing to changes in microstructure. Therefore, the crack could advance around intact regions and leave behind 'pinning' ligaments (illustrated in Figure 6(b)). The SRCT data also evidenced that smaller/thinner bridging ligaments formed from the bulk epoxy were more likely to deform inelastically (shown in Figure 7), with thicker ligaments fracturing prior to substantial deformation. It is thought that the thinner ligaments facilitate additionally energy absorbance through maintaining traction forces across the crack flanks more effectively and to a greater extent. Many authors also postulate that the de-bonding particles facilitate the transition of plane-strain to plane-stress within the ligaments, allowing for deformation/toughening processes [11]. Therefore, a 3D model would be required to capture this geometry, and hence, enable the behaviour of the constituent resin to be captured (assuming the material properties in the model are well defined).

Another key limitation of the models was due to the lack of measured material properties at the micro-scale. This was less critical for the parametric studies conducted here, but will need to be considered in the future. Currently, the resin material definition is essentially elastic and does not account for the visco-elastic/visco-plastic behavior as mentioned previously. Additionally, in this first instance, the interface strengths were assumed equal in the normal and shear directions, but it is acknowledged that this is not representative of reality. Nonetheless, the simulations have permitted a number of recommendations to be made to the manufacturer with regards to the relative strengths of the fibre and particle interface strengths, and with regards to the sensitivity of the crack path to a non-uniform distribution of particles. This sensitivity of the crack path to the local particle distribution is emphasized in Figure 8, where the crack path preferentiality was captured both experimentally and in the models. It is clear that image-based models provide the opportunity to incorporate realistic microstructures into FE simulations, which is being increasingly exploited in the composites field [12], [13], while the time-resolved data gives the possibility of some form of direct validation, which could be via internal strain mapping [4], [14] and crack path comparisons.

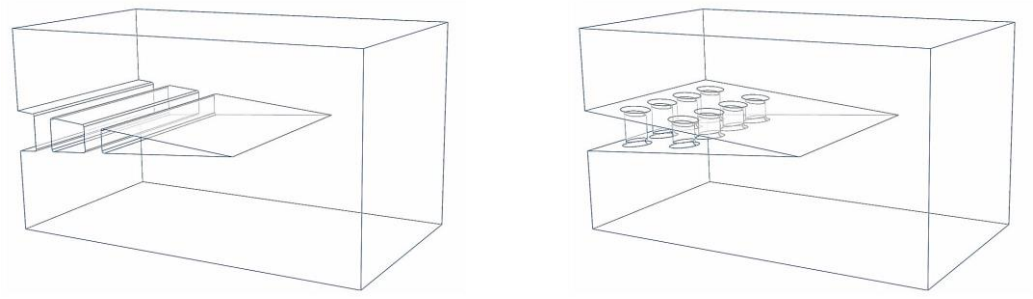

(a) (b)

Figure 6: Sketch of the key differences between; (a) a plane-strain model, and (b) a more representative 3D geometry

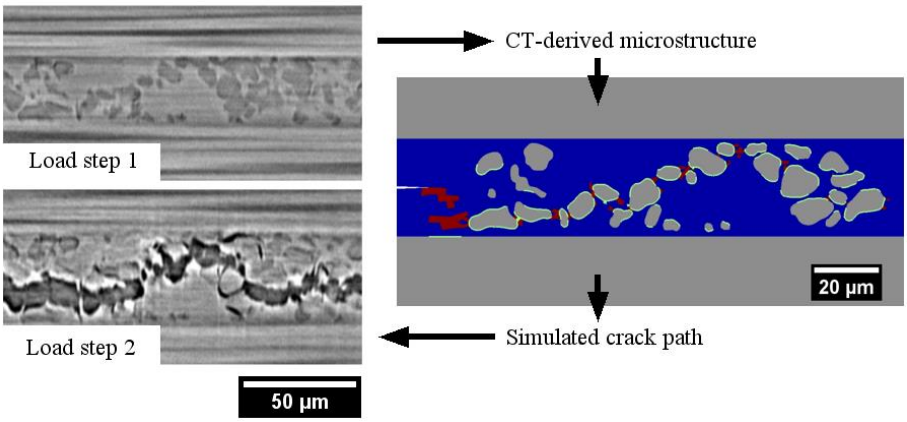

Figure 7: A simulated crack path supported by the time-resolved CT data that showed that the crack path preferentially follows the de-bonding particles, with the additional observation that the thin bridging ligaments formed from epoxy resin are capable of substantial deformation, which is not captured in the FE simulations

5 CONCLUSIONS

Overall, the presented work has shown that image-based FE models can be initialised and validated (to a certain extent) by time-resolved CT data. The models also show that fibre interface failure precedes the crack path propagating towards it, supporting the idea that the crack path through the interlayer is initiation controlled. Therefore, it is important to control the peak stresses along the fibre interfaces through control over the interlayer constituents, which in these models could be achieved with de-bonding particles. These de-bonding particles serve to relieve the stresses ahead of the contiguous crack tip and also facilitate the formation of bridging ligaments through the discontinuous nature of the crack tip process zone. As expected, an interlaminar crack path is also promoted when the fibre interface strength is high. Experimentally, it was observed that large particle-depleted regions may also trigger failure at the fibre interfaces, which was also replicated in the simulations. The trends identified in the parametric study may be used by manufacturers to target a balance between too easily de-bonding particles (that may be detrimental to other properties), while particles that adhere too well to the resin may trip failure along the fibre interfaces. In the future, it is expected that the computational expense of 3D models with multiple interacting cracks will reduce, allowing the geometry of the resin bridging ligaments to be captured more faithfully and with non-linear material properties, therefore allowing some of these ligaments to be preserved further into the crack wake.

ACKNOWLEDGEMENTS

The authors acknowledge contributions from institutions and staff: Solvay, the Impact Acceleration Accounts funding from the Engineering and Physical Sciences Research Council, the µ-VIS Centre at the University of Southampton, and the Swiss Light Source and funding from the Community's Seventh Framework Programme (FP7/2007-2013).

REFERENCES

[1] M. O. W. Richardson and M. J. Wisheart, Review of low-velocity impact properties of composite materials, *Composites Part A: Applied Science and Manufacturing*, **27**, 1996, pp. 1123–1131.

[2] D. J. Bull, A. E. Scott, S. M. Spearing, and I. Sinclair, The influence of toughening-particles in CFRPs on low velocity impact damage resistance performance, *Composites Part A: Applied Science and Manufacturing*, **58**, 2014, pp. 47–55.

[3] G. Borstnar, M. N. Mavrogordato, L. Helfen, I. Sinclair, and S. M. Spearing, Interlaminar fracture micro-mechanisms in toughened carbon fibre reinforced plastics investigated via synchrotron radiation computed tomography and laminography, *Composites Part A: Applied Science and Manufacturing*, **71**, 2015, pp. 176-183.

[4] G. Borstnar, F. Gillard, M. N. Mavrogordato, I. Sinclair, and S. M. Spearing, Three-dimensional deformation mapping of Mode I interlaminar crack extension in particle-toughened interlayers, *Acta Materialia*, **103**, 2016, pp. 63-70.

[5] M. Hojo, S. Matsuda, M. Tanaka, S. Ochiai, and A. Murakami, Mode I delamination fatigue properties of interlayer-toughened CF/epoxy laminates, *Composites Science and Technology*, vol. **66**(5), 2006, pp. 665–675.

[6] N. Sela and O. Ishai, Interlaminar fracture toughness and toughening of laminated composite materials: A review, *Composites*, **20**(5), 1989, pp. 423–35.

[7] G. Borstnar, M. N. Mavrogordato, Q. D. Yang, I. Sinclair, and S. M. Spearing, Crack path simulation in a particle-toughened interlayer within a polymer composite laminate, *Composites Science and Technology*, **133**, 2016, pp. 89–96.

[8] Y. Xie and M. Koslowski, Numerical simulations of inter-laminar fracture in particle-toughened carbon fiber reinforced composites, *Composites Part A: Applied Science and Manufacturing*, **92**, 2016, pp. 62-69.

[9] P. Cloetens, M. Pateyron-Salomé, J. Y. Buffière, G. Peix, J. Baruchel, F. Peyrin, and M. Schlenker, Observation of microstructure and damage in materials by phase sensitive radiography and tomography, *Journal of Applied Physics*, **81**(9) 1997, pp. 5878.

[10] F. Marone and M. Stampanoni, GRIDREC software, *Journal of Synchrotron Radiation.*, **19**, 2012, pp. 1029–1037.

[11] R. Bagheri, B. T. Marouf, and R. A. Pearson, Rubber-Toughened Epoxies: A Critical Review, *Polym. Reviews*, **49**(3), 2009, pp. 201–225.

[12] L. P. Djukic, G. M. Pearce, I. Herszberg, M. K. Bannister, and D. H. Mollenhauer, Contrast Enhancement of MicroCT Scans to Aid 3D Modelling of Carbon Fibre Fabric Composites, *Applied Composite Materials*, **20**(6), 2013, pp. 1215–1230.

[13] I. Straumit, S. V. Lomov, and M. Wevers, Quantification of the internal structure and automatic generation of voxel models of textile composites from X-ray computed tomography data, *Composites Part A: Applied Science and Manufacturing*, **69**, 2015, pp. 150–158.

[14] R. Brault, A. Germaneau, J. C. Dupré, P. Doumalin, S. Mistou, and M. Fazzini, In-situ Analysis of Laminated Composite Materials by X-ray Micro-Computed Tomography and Digital Volume Correlation, *Experimental Mechanics*, **53**, 2013, pp.1143.